International Journal of Computer Science and Information Technology
ISSN: 3005-9682 (Print), ISSN: 3005-7140 (Online) | Volume 7, Number 3, Year 2025
DOI: https://doi.org/10.62051/ijcsit.v7n3.03
Journal homepage: https://wepub.org/index.php/IJCSIT/index

Optically-Integrated Microfluidic Tweezer Sensor

Zhaotong Song [1], Cun Zhao [1,*], Binhai Zhu [2]

[1] College of Electrical and Information Engineering, Northeast Petroleum University, Daqing 163318, China

[2] School of Intelligent Manufacturing Engineering, Harbin Huade University, Harerbin 150025, China

*Corresponding Author: zhaocun_nepu@163.com

ABSTRACT

Liquid viscosity measurement plays a crucial role in biomedical and clinical diagnostics. However, conventional viscosity measurement techniques face risks of cell damage and sample contamination in biomedical applications. In this study, we propose a liquid viscosity sensor that integrates microfluidic technology with fiber-optic tweezers. The sensor captures cells in a non-contact manner using optical tweezers and measures viscosity by analyzing the cells' dynamic response under viscous drag. When the liquid flows, the trapped cells exhibit microscale displacements within the optical trap, which are directly related to the liquid viscosity.

KEYWORDS

Fiber-optic tweezers; Microfluidics; Liquid viscosity sensing

1. INTRODUCTION

Viscosity is a fundamental parameter for characterizing the properties of fluids [1]. Accurate measurement of liquid viscosity is of paramount importance in a wide range of fields, including biomedical research [2-4], materials science and chemical engineering [5, 6] , and industrial production [7]. In biological systems in particular, changes in liquid viscosity are often closely associated with the microenvironment surrounding cells [8], cellular physiological states [9], and the occurrence and progression of diseases [10]. For example, the viscosity coefficient of blood, a biological fluid, is a key indicator of health assessment [11]. Elevated blood viscosity serves as a predictive marker for cardiovascular diseases, and the effectiveness of triglyceride drugs in preventing such diseases can be determined by monitoring changes in blood viscosity. Extracellular fluid (ECF) viscosity, as a physical cue in the cellular microenvironment, can influence cell migration, proliferation, differentiation, and morphology, and its alterations are associated with diseases like inflammation and cancer [12]. Therefore, developing a liquid viscosity measurement technique that is accurate, non-destructive, and suitable for complex biological environments has become one of the current research frontiers.

2. THEORETICAL ANALYSIS

Based on the coupling principle of optical trapping mechanics and fluid dynamics, the proposed system realizes liquid viscosity sensing through non-contact optical manipulation. As shown in Figure. 1, when a cell is trapped at the tip of the fiber probe, the optical force acting on it consists of two components: the axial gradient force $F_{sc,z}$ and the scattering force F_{gr}. Along the fiber axis (Z-

axis), the gradient force $F_{sc,z}$ pulls the cell toward the fiber end face, while the scattering force F_{gr} pushes the cell away from the fiber. A stable three-dimensional optical potential well is formed when these two forces reach dynamic equilibrium. In the direction perpendicular to the fiber axis (Y-axis), the cell is subjected to the gradient force $F_{sc,y}$. When the trapped cell experiences the viscous drag force $F_{viscous}$, the gradient force $F_{sc,y}$ prevents the cell from escaping the optical trap.

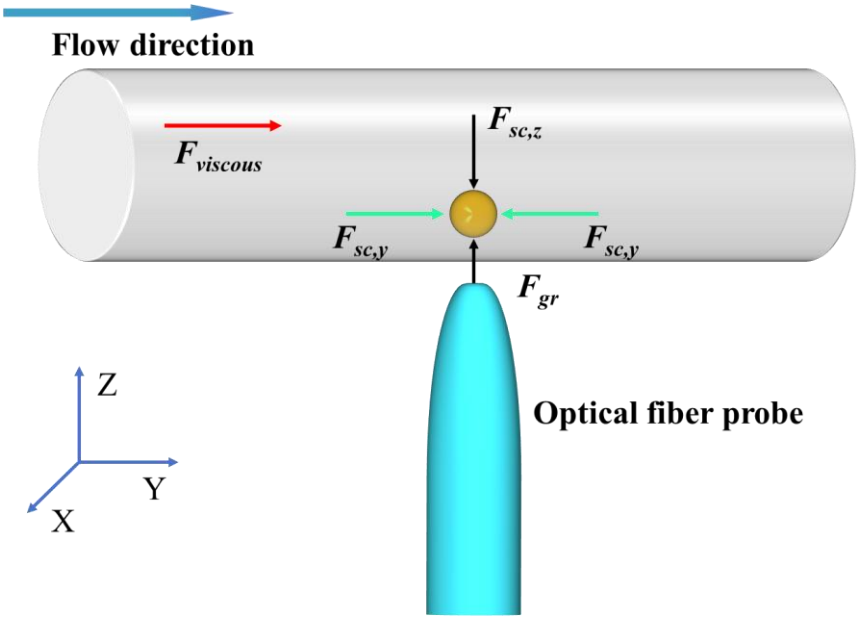

Figure 1. Schematic force analysis of a cell trapped by the fiber-optic tweezers

Therefore, once the cell is stably trapped in the optical potential well, liquids with different viscosity coefficients flow at the same velocity, and the trapped cell is simultaneously subjected to the viscous drag force $F_{viscous}$. The viscous drag force $F_{viscous}$ can be expressed as:

$$F_{viscous} = 6\pi\eta r v_1 \tag{1}$$

Where $F_{viscous}$ denotes the viscous drag force, η is the liquid viscosity coefficient, r is the cell radius (assuming the yeast cell is spherical), and v_1 represents the liquid flow velocity. Accordingly, the viscosity coefficient η can be derived as:

$$\eta = \frac{F_{viscous}}{6\pi r v_1} \tag{2}$$

When the viscous drag force acts on the cell trapped in the optical potential well, the cell is displaced to an offset position Δx from the trap center. The velocity of the cell is denoted as v_2 (with $v_1 \approx v_2$), and equilibrium is reached at the new position, where $F_{viscous} = F_O$. At this point, the optical force can be expressed as $F_O = -k\Delta x$. Substituting into Eq. (2), the liquid viscosity coefficient η can be approximately expressed as:

$$\eta = \frac{F_O}{6\pi r v_1} \approx \frac{k\Delta x}{6\pi r v_2} \approx \frac{k\Delta t}{6\pi r} \tag{3}$$

Δt denotes the time corresponding to the change in backscattered light caused by the oscillation of the cell within the optical trap. Accordingly, the backscattered light variation time Δt is approximately proportional to the liquid viscosity coefficient:

$$\Delta t \propto \eta \tag{4}$$

Therefore, by measuring the variation time of the backscattered light signal, the viscosity coefficient of the fluid can be indirectly determined. Meanwhile, when the fiber-optic tweezers stably trap a cell, a portion of the backscattered light is coupled back into the fiber, and the backscattered light intensity is significantly enhanced. When the trapped cell undergoes a slight displacement within the optical trap, the backscattered light intensity decreases. Accordingly, the sensor's output signal exhibits a negative step-like response.

3. NUMERICAL SIMULATION

Theoretical models for analyzing the forces acting on particles trapped in optical tweezers are generally divided into geometric optics models and electromagnetic field models. Since the radius of the trapped cells in the experiment, r ($r = 5\ \mu m$), is much larger than the wavelength of the laser used, λ ($\lambda = 980\ nm$), the cells fall into the Mie particle regime and satisfy the Mie scattering condition, so the geometric optics model should be used for calculations. In this study, we employ finite element analysis based on Maxwell's equations to precisely describe the distribution and variation of the vector optical field. The optical force F_O acting on the trapped cell is given by:

$$F_O = \oint_V \nabla \cdot \mathrm{T} dV = \oint_S (< TM > \cdot \mathrm{n}) dS \tag{5}$$

In the equation, the integration is performed over the closed surface S surrounding the particle, ∇ denotes the gradient operator, n is the surface normal vector, and $\langle TM \rangle$ represents the time-averaged Maxwell stress tensor, which can be calculated according to Eq. (6):

$$< TM > = \frac{1}{2} Re[\varepsilon EE^* + \mu HH^* - \frac{1}{2}(\epsilon |E|^2 + \mu |H|^2) I] \tag{6}$$

In the equation, E denotes the electric field, H denotes the magnetic field, $EE^*$and HH^* represent the outer products of the electromagnetic fields, ε is the permittivity of the surrounding medium, μ is the permeability, and I denotes the identity dyad.

To evaluate the trapping capability of the fiber-optic tweezers for cells within the microfluidic channel, a two-dimensional finite element method (TEM) model was established using the Electromagnetic Waves, Frequency Domain module in COMSOL Multiphysics. Numerical simulations were conducted to analyze the optical field distribution and the optical forces acting on the cell during trapping. The simulation setup is illustrated in Figure. 2. Yeast cells with a diameter of 5 μm and a refractive index of 1.39 were considered. The fiber was exposed to air with a refractive index of 1, while the microfluidic channel was filled with water, with a refractive index of 1.33. The refractive indices of the fiber probe and the microfluidic channel were set to 1.45.

The distance from the fiber probe to the outer wall of the microfluidic channel was 2 μm, with a wall thickness of 1 μm, and the input power was set to 25 mW. As shown in Fig. 2(b), the electric field intensity along the X-axis cross-section indicates that the cell is trapped at X = 22.85 μm. Figure. 2(c) shows the optical force acting on the cell along the Y-axis at X = 22.85 μm. As the cell approaches the optical axis (Y = 0 μm), F_Y gradually increases, reaches a maximum, and then rapidly decreases to zero. Therefore, the cell can be firmly trapped along the optical axis by the fiber probe. Analysis along both the X and Y axes confirms that the particle reaches equilibrium at the designated position.

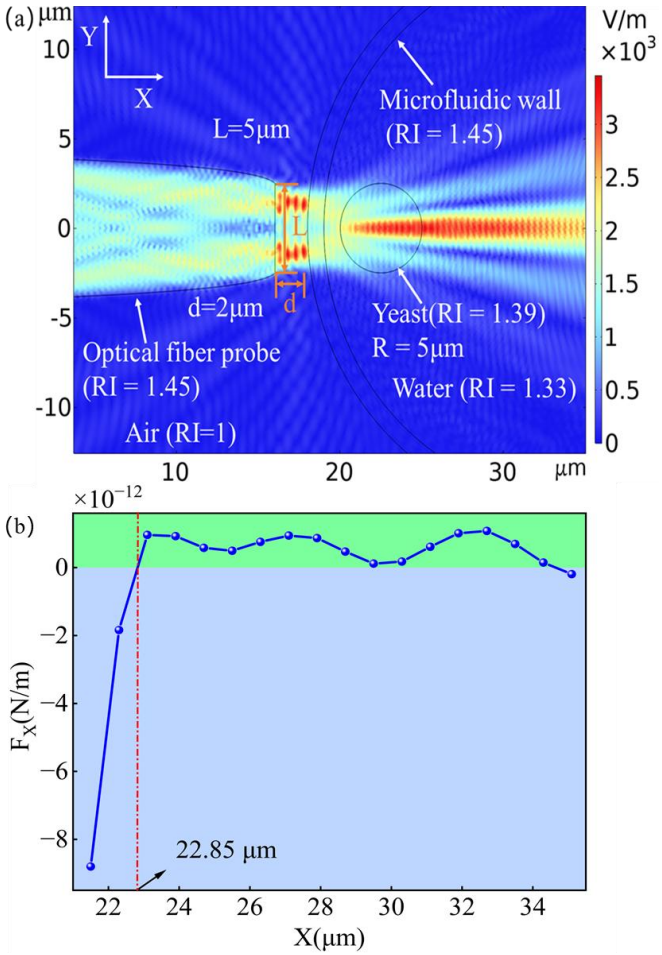

Figure 2. Electric field distribution and simulated optical forces. (a) Electric field distribution of a cell trapped in the microfluidic channel by the fiber probe. (b) Optical force on a yeast cell along the X-axis within the microfluidic channel.

When light enters the microfluidic channel from the fiber probe, refraction and reflection occur due to the curved structure of the microcapillary walls. The curvature of the microfluidic channel walls acts like a lens, providing secondary focusing of the light beam and enhancing the interaction between light, the cell, and the surrounding fluid. To verify this hypothesis, we performed simulations to calculate the optical forces under different environmental conditions. As shown in Figure. 3(a), along the X-axis, a sample in a conventional sample chamber experiences only scattering forces and cannot be trapped. The optical force on the cell in the microfluidic channel increased from $7.60\times10^{-12}\ N/m$ on a planar glass substrate to $8.80\times10^{-12}\ N/m$, an increase of approximately 1.16 times. Along the Y-axis, compared with the planar glass substrate, the microfluidic channel increased the optical force from $9.6\times10^{-12}\ N/m$ to $1.15\times10^{-11}\ N/m$, an increase of 1.20 times.Compared with the optical force in a conventional sample chamber ($7.86\times10^{-12}\ N/m$), this represents an increase of 1.46 times.

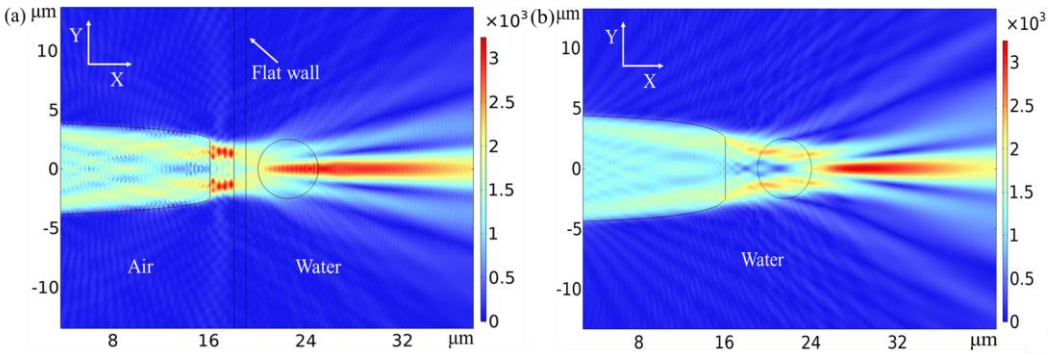

Figure 3. Electric field distribution and simulated optical forces under different conditions. (a) Electric field intensity for a planar glass substrate of the same thickness. (b) Electric field intensity in a conventional sample chamber.

4. SUMMARY

In summary, this work proposes a liquid viscosity sensor that combines microfluidics with fiber-optic optical tweezers. A 980 nm laser is used to form an optical trap at the focal point of the capillary lens, enabling the capture of micrometer-scale cells. As the viscosity coefficient increases, the displacement of the cell within the optical trap increases, leading to a longer variation time of the backscattered light signal, thereby enabling sensing of the liquid viscosity coefficient.

REFERENCES

[1] KIM B J, LEE S Y, JEE S, et al. Micro-Viscometer for Measuring Shear-Varying Blood Viscosity over a Wide-Ranging Shear Rate [J]. Sensors, 2017, 17(6): 1442.

[2] EIDI A. Blood Viscosity Biosensor Based on Electromagnetic Resonator [J]. Cardiovascular Engineering and Technology, 2023, 14(4): 526-533.

[3] KWAPISZEWSKA K, SZCZEPANSKI K, KALWARCZYK T, et al. Nanoscale Viscosity of Cytoplasm Is Conserved in Human Cell Lines [J]. Journal of Physical Chemistry Letters, 2020, 11(16): 6914-6920.

[4] KALWARCZYK T, ZIEBACZ N, BIELEJEWSKA A, et al. Comparative Analysis of Viscosity of Complex Liquids and Cytoplasm of Mammalian Cells at the Nanoscale [J]. Nano Letters, 2011, 11(5): 2157-2163.

[5] OU H Y, SU L, SHI Y, et al. Investigation on High-Viscosity Chemical Waste Liquid Atomizer Based on VOF-DPM [J]. Energies, 2023, 16(7): 3109.

[6] ZHU A L, WANG J J, HAN L J, et al. Measurements and correlation of viscosities and conductivities for the mixtures of imidazolium ionic liquids with molecular solutes [J]. Chemical Engineering Journal, 2009, 147(1): 27-35.

[7] Kielczynski P, Szalewski M, Balcerzak A, et al. Density and viscosity of liquids determination using an inverse method for Love wave propagation [C]//2014 IEEE International Ultrasonics Symposium. IEEE, 2014: 1992-1995.

[8] LABORIE E, MELCHIONNA S, STERPONE F. An operative framework to model mucus clearance in silico by coupling cilia motion with the liquid environment [J]. The Journal of Chemical Physics, 2023, 158(9).

[9] HERMANS E, VERMANT J. Interfacial shear rheology of DPPC under physiologically relevant conditions [J]. Soft Matter, 2014, 10(1): 175-86.

[10] NARDINI M, CIASCA G, LAURIA A, et al. Sensing red blood cell nano-mechanics: Toward a novel blood biomarker for Alzheimer's disease [J]. Frontiers in Aging Neuroscience, 2022, 14: 932354.

[11] ROSENSON R S, SHOTT S, TANGNEY C C. Hypertriglyceridemia is associated with an elevated blood viscosity Rosenson: triglycerides and blood viscosity [J]. Atherosclerosis, 2002, 161(2): 433-439.

[12] LI Y, LIU N, XIE N, et al. Extracellular fluid viscosity: a new physical cue in cell biology [J]. Acta Mechanica Sinica, 2024, 40(5): 624056.